Nonlinear detection of paleoclimate-variability transitions possibly related to human evolution

Jonathan F. Donges[a,b,1], Reik V. Donner[a,c], Martin H. Trauth[d], Norbert Marwan[a], Hans-Joachim Schellnhuber[a], and Jürgen Kurths[a,b,e]

[a]Potsdam Institute for Climate Impact Research, Potsdam, Germany; [b]Department of Physics, Humboldt University, Berlin, Germany; [c]Institute for Transport and Economics, Dresden University of Technology, Dresden, Germany; [d]Department of Earth and Environmental Sciences, University of Potsdam, Potsdam, Germany; and [e]Institute for Complex Systems and Mathematical Biology, University of Aberdeen, Aberdeen AB24 3FX, United Kingdom

Contributed by Hans-Joachim Schellnhuber, October 18, 2011 (sent for review July 27, 2011)

Potential paleoclimatic driving mechanisms acting on human evolution present an open problem of cross-disciplinary scientific interest. The analysis of paleoclimate archives encoding the environmental variability in East Africa during the past 5 Ma has triggered an ongoing debate about possible candidate processes and evolutionary mechanisms. In this work, we apply a nonlinear statistical technique, recurrence network analysis, to three distinct marine records of terrigenous dust flux. Our method enables us to identify three epochs with transitions between qualitatively different types of environmental variability in North and East Africa during the (*i*) Middle Pliocene (3.35–3.15 Ma B.P.), (*ii*) Early Pleistocene (2.25–1.6 Ma B.P.), and (*iii*) Middle Pleistocene (1.1–0.7 Ma B.P.). A deeper examination of these transition periods reveals potential climatic drivers, including (*i*) large-scale changes in ocean currents due to a spatial shift of the Indonesian throughflow in combination with an intensification of Northern Hemisphere glaciation, (*ii*) a global reorganization of the atmospheric Walker circulation induced in the tropical Pacific and Indian Ocean, and (*iii*) shifts in the dominating temporal variability pattern of glacial activity during the Middle Pleistocene, respectively. A reexamination of the available fossil record demonstrates statistically significant coincidences between the detected transition periods and major steps in hominin evolution. This result suggests that the observed shifts between more regular and more erratic environmental variability may have acted as a trigger for rapid change in the development of humankind in Africa.

African climate | Plio-Pleistocene | climate-driven evolution | dynamical transitions | nonlinear time series analysis

Recent comparisons of terrestrial and marine paleoclimate archives have resulted in an intense debate concerning global vs. regional forcing of East Africa's climate and its relationship to human evolution during the past 5 Ma (1–4). The gradual long-term retreat of equatorial rain forests and the emergence of drier environments in East Africa (2, 5, 6) were interrupted by distinct epochs of increased humidity indicated by paleo-lake levels in different basins of the East African Rift System (EARS) displaying synchronous highs at about 2.7–2.5, 1.9–1.7, and 1.1–0.9 Ma B.P. (7). Notably, these epochs coincide well with certain global-scale climate transitions like the final closure of the Panama isthmus (8–10), intensification of the atmospheric Walker circulation (11), and the shift from a predominance of obliquity-driven glacial variability (41 ka period) to glacial-interglacial cycles with a 100 ka period (12, 13). Further reconstructions revealed additional relevant lake periods at 4.7–4.3, 4.0–3.9, 3.4–3.3, and 3.2–2.95 Ma B.P. (3). Previous findings suggest that the dominating summer aridity in the East African climate was controlled mainly by orbitally driven changes in the local irradiation driving regional monsoon activity via changes of sea-surface temperatures (SSTs) (5, 14–18) rather than by high-latitude glacial dynamics. In addition, tectonic activity and the resulting complex topography of East Africa could have triggered particularly variable climate conditions during the Plio-Pleistocene (18, 19).

As early as Darwin (20), scholars have speculated on if and how climate change shaped human evolution (4). On the basis of the present-day knowledge of the Plio-Pleistocene African climate, three general hypotheses concerning mechanisms of climate-induced mammalian evolutionary processes are currently discussed (18): (*i*) The *turnover pulse hypothesis* postulates progressive habitat changes (21, 22) due to abrupt climate shifts (1, 2) enforcing the adaptation of existing and the evolution of new species. (*ii*) The *variability selection hypothesis* proposes an increasing instability of environmental conditions as a driver for the simultaneous emergence of species (23, 24). (*iii*) Finally, the *pulsed climate variability hypothesis* promotes spikes of more variable climate conditions unrelated to high-latitude glacial cycles as a key driver of evolutionary selection (3, 6, 7, 25). With the currently available paleoclimate and paleoanthropological records, it has not been possible to provide clear evidence for one of these hypotheses by means of traditional (linear) statistical analysis.

Although there is an unequivocal correlation of terrestrial and marine paleoclimate records, to date, marine sediments (Fig. 1) provide the only archive that allows the study of the Plio-Pleistocene African climate on all relevant time scales. However, earlier analyses of terrigenous dust flux records using traditional time series analysis techniques to detect important transitions in the African climate yielded contradictory results with respect to the signature and timing of these events (1, 2, 17). Difficulties like these are to be expected when applying linear methods to the highly nonlinear climate system underlying paleoclimate proxy records. Linear techniques of time series analysis by definition are limited to the study of linear dynamics. To circumvent this problem and explore the vast remainder of nonlinear phenomena, here we present results on the basis of a nonlinear method of time series analysis, recurrence network (RN) analysis (see *SI Text*). RN analysis enables us to reliably detect qualitative changes within observational time series, which are largely indiscernible for linear methods of data analysis (26–28). This instrument leads to an improved detection of a particular flavor of Plio-Pleistocene African climate change and its potential influence on the habitats of early humans. On the basis of concepts of dynamical systems and graph theory, RN analysis is particularly efficient in applications where the number of observations is limited and the data points are unevenly spaced, which is common for paleoclimate proxy records such as time series of dust accumulation rates (29).

Author contributions: J.F.D., R.V.D., M.H.T., H.-J.S., and J.K. designed research; J.F.D. and R.V.D. performed research; J.F.D., R.V.D., and N.M. contributed new reagents/analytic tools; J.F.D. and R.V.D. analyzed data; and J.F.D., R.V.D., M.H.T., and H.-J.S. wrote the paper.

The authors declare no conflict of interest.

Freely available online through the PNAS open access option.

[1]To whom correspondence should be addressed. E-mail: donges@pik-potsdam.de.

This article contains supporting information online at www.pnas.org/lookup/suppl/doi:10.1073/pnas.1117052108/-/DCSupplemental.

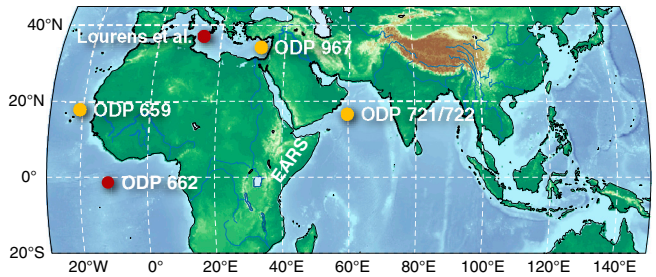

Fig. 1. Map displaying the locations of the marine sediment cores analyzed in this study (orange): ODP 659 (East Atlantic) (34), 721/722 (Arabian Sea) (1, 2), and 967 (Eastern Mediterranean Sea) (66). In addition, locations of additional complementary records of Plio-Pleistocene climate evolution (red) in the Atlantic [ODP site 662 (61)] and the Mediterranean [composite sequence of marine sediments at the Sicilian and Calabrian coast (69)] as well as the EARS are shown.

Specifically, RN analysis is sensitive to general changes in the dynamics rather than those in the amplitudes of the entire record (e.g., trends in mean or variance) or modes with a certain periodicity. Therefore it is well suited for detecting tipping points or, more generally, bifurcations in the behavior of nonlinear complex systems like Earth's climate (28–30).

Results

For detecting significant shifts in the dynamics of Plio-Pleistocene African climate as reflected by terrigenous dust flux (see *Materials and Methods*), we rely on two established measures of complex network theory: transitivity and average path length (31). It has been theoretically and empirically shown in several studies that, when calculated for RNs of selected time series segments (see *SI Text*), transitivity reflects the regularity of the dynamics within this segment or time window (28, 30, 32). Noisy or chaotic dynamics gives rise to low values, whereas (almost) periodic or laminar behavior induces high values of transitivity. We therefore refer to it as a climate regularity (CR) index in the following. Along the same lines, extreme values of the average path length indicate an abrupt dynamical change (ADC) between different dynamical regimes within the considered time window (28, 30, 32) (see *SI Text*). It is a crucial feature of our approach that CR and ADC do not reflect changes in long-term trends but are, in contrast, sensitive to the regularity of short-term fluctuations (CR) and general abrupt changes in this short-term dynamics (ADC). Both measures are hence responsive to different nonlinear aspects of the time series data and do not necessarily show transitions at the same epochs (27, 29, 30). If they do so, however, this double-evidence points at a particularly relevant feature in the data.

For representative dust flux records from the Atlantic as well as the Indian Ocean [Ocean Drilling Program (ODP) sites 659 and 721/722, Fig. 2*A*], CR reveals surprisingly similar long-term change in short-term fluctuations before about 1.5 Ma B.P. (in contrast to the Mediterranean ODP site 967, Fig. 2*A*), although both sites are strongly geographically separated and, hence, characterized by distinct wind systems and dust sources (1, 17, 33) (Fig. 2*B*). Specifically, the Saharan Air Layer, African Equatorial Jet, and trade winds contribute at ODP site 659 (34), whereas the Shamal winds from the Arabian Peninsula, which are connected to the western branch of the Asian monsoon system, dominate at ODP site 721/722 (35). This overall picture indicates that changes in CR during the Pliocene and early Pleistocene are robust manifestations of long-term variations in the dynamics of large-scale African dust mobilization and transport.

As a particularly striking feature, we identify a pronounced maximum of CR between 3.5 and 3.0 Ma B.P. at both ODP sites 659 and 721/722 signaling a period of exceptionally regular dust flux dynamics. The epochs highlighted by ADC support these findings (Fig. 2*C*). The time interval 3.5–3.0 Ma B.P. is characterized by three distinct and highly significant extrema (two maxima and one minimum) in the ODP site 659 record, indicating shifts between regimes of higher and lower regularity in the variations

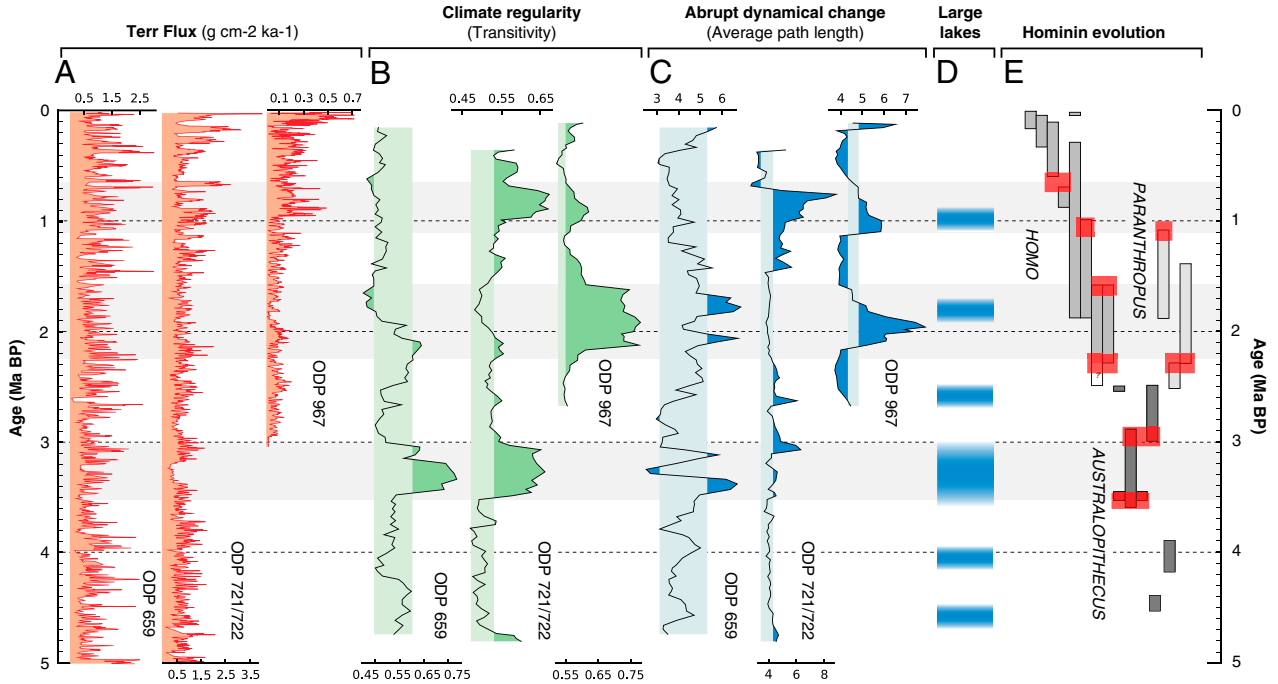

Fig. 2. (*A*) Terrestrial dust flux records from the three considered ODP sites (1, 2, 34, 66). (*B*,*C*) Results of RN analysis of the three dust flux records including 90% confidence bands (vertical shadings) of a stationarity test (*SI Text*). Comparing both measures for all records reveals significant and synchronous large-scale regime shifts in dust flux dynamics (horizontal shadings). (*D*) Time intervals with geological evidence for large lakes in East Africa, comprising collected information from different areas in the EARS (3) and additional results from the Afar basin (65, 70). (*E*) Major known steps of human evolution in East Africa (simplified from ref. 3). Red bars indicate epochs where the possible emergence and/or extinction of known hominin species coincides with detected climate transitions (*SI Text*).

of environmental conditions (30). Similar observations can be made for the ODP site 721/722 data; however, the increased values of ADC are less well pronounced but persist considerably longer (until 2.8 Ma B.P.).

In general, the variations of ADC observed at ODP sites 659 and 721/722 differ remarkably (Fig. 2*C*), although CR traces consistent shifts between more and less regular variability until about 1.5 Ma B.P. By considering the Mediterranean record (ODP site 967), further synchronous events are identified. Specifically, we find an extended, highly significant maximum of CR between about 2.25 and 1.6 Ma B.P. and of ADC between 2.2 and 1.7 Ma B.P. The latter one roughly coincides with the observations made at ODP site 659. Moreover, between about 1.1 and 0.7 Ma B.P., both CR and ADC show significant maxima for ODP site 967 and ODP site 721/722 but not for ODP site 659.

In summary, our analysis identifies three main epochs of interest: 3.5–3.0, 2.25–1.6, and 1.1–0.7 Ma B.P. (Fig. 2). All three are characterized by significant extrema of CR and/or ADC in at least two of the analyzed records. In addition, there are further shorter time periods of considerably increased or decreased CR or ADC observed in different records which are, however, typically less pronounced. Our results do not change significantly if the basic parameters of our analysis method (see *SI Text*) are modified (29).

Discussion

Nonlinear Identification of Critical Transitions in Paleoclimate. Tipping points in the climate system—i.e., values of system parameters at which critical transitions in climate dynamics take place—have gained increasing attention in the course of the ongoing debate on potential impacts of anthropogenic climate change (36–38). Given the large risk (product of impact and likelihood) associated with the activation of certain climate tipping elements (e.g., the Greenland and West Antarctic ice sheets), understanding and anticipating future qualitative changes in climate tipping elements is of major importance and requires a good knowledge of past transitions recorded in paleoclimate data (39). Previous research revealed precursory signatures associated with climate tipping points (39–41). Predominantly, changes in the variance structure of characteristic observables represent a critical slowing down of intrinsic transient responses within the data prior to the instabilities (42–46).

RN analysis is a promising exploratory tool for detecting structural changes in paleoclimate dynamics potentially associated with certain tipping elements in Earth's climate system. It has several advantages above other frequently used techniques for detecting (incipient) bifurcations in time series: (*i*) RN analysis is *not* explicitly based on temporal correlations but on geometric considerations (47). Hence it is more robust with respect to noisy and nonuniformly sampled paleoclimate time series with uncertain timing than methods relying on temporal correlations (42–44, 48) like degenerate fingerprinting (42) and detrended fluctuation analysis (43). (*ii*) As a nonlinear technique, RN analysis is not restricted to detecting only changes in linear statistical properties (i.e., the autocovariance structure) of a time series (42, 44–46). In contrast, it characterizes more general variations in the recorded dynamics, which may become particularly relevant close to bifurcation points. (*iii*) RN analysis has been shown to reliably perform with a comparably small number of data points (29, 32), particularly when contrasting it with linear spectral methods (1, 2) or certain nonlinear stochastic models of climate fluctuations for detecting noisy bifurcations (49, 50).

We emphasize that all existing methods for detecting tipping points from paleoclimate time series (including RN analysis) make use of sliding window techniques. By construction, such methods have a limited temporal resolution of the variations of the statistics of interest. Hence, identified dynamical transitions can be attributed only to epochs rather than distinct points in time. This strategy has the advantage of a higher robustness with respect to uncertainties in the data themselves as well as the associated age models, rendering the results of RN analysis particularly robust and statistically reliable (29).

Climatological Interpretation. The three identified transition periods (Fig. 2), which are only partially known from previous studies, can be clearly related to distinct and known climatic mechanisms. Specifically, the interval 1.1–0.7 Ma B.P. corresponds to the Middle Pleistocene transition (MPT) characterized by a change from glacial cycles predominantly related to obliquity variations of Earth's orbit (approximately 41 ka period) to such with an approximately 100 ka periodicity. The timing of this transition and its underlying mechanisms have been extensively studied elsewhere (13, 51). That the MPT is not detected in the record from ODP site 659 by RN analysis does not imply that it did not have any climatic impact in the corresponding dust-source areas in Northwest Africa. It just shows that our technique is not sensitive to the local signature of the transition, if present, e.g., if it manifests itself in some change of trend (1, 2, 17) (see the discussion in *Results*). Alternatively, the locally available data may be insufficient in quality and/or resolution to reveal the subtle type of events RN analysis is focusing on. This reasoning holds for any other known transition that is not detected by our method in any of the considered records. Regarding the transition period in the Early Pleistocene (2.25–1.6 Ma B.P.), the timing well coincides with known large-scale changes in atmospheric circulation associated with an intensification and spatial shift of the Walker circulation (11).

The third identified transition period includes the Middle Pliocene (3.3–3.0 Ma B.P.), the last long period during which global mean temperatures have been consistently higher than present day (52). This epoch is thus considered as an analog for the future climate of the late 21st century if anthropogenic emissions of greenhouse gases continue to rise (53). It was characterized by a strongly reduced meridional temperature gradient due to an intermittent poleward shift of the North Atlantic overturning resulting in a strong warming of the Arctic by oceanic surface currents (54, 55). At the same time, RN analysis reveals an enhanced regularity of African dust flux variations in both the Arabian Sea and Atlantic Ocean. At ODP site 721/722, this observation is predominantly caused by a well-pronounced epoch of relatively weak and approximately constant dust flux between about 3.36 and 3.17 Ma B.P. (Fig. 3*E*). A similar—but shorter—feature is found at ODP site 659 between about 3.25 and 3.19 Ma B.P. (Fig. 3*D*) as well as at ODP sites 661 and 662 in the Eastern Equatorial Atlantic (1, 2). The presence of such very similar features with a clearly different timing suggests the presence of either one common climatological mechanism influencing the Arabian Peninsula *much earlier than* Northwest Africa or two distinct (but eventually interrelated) factors, where the first affected only the Northeast African and/or Arabian dust flux dynamics.

A first important candidate factor is the marine isotope stage (MIS) M2 (56), an unusually cold period (3.32–3.28 Ma B.P.) prior to the Middle Pliocene warm period (57, 58); cf. Fig. 3*A*. This cooling was most likely triggered by a significant reduction of northward heat transport via the North Atlantic Current between 3.33 and 3.283 Ma B.P. (59)—possibly due to intermittent closures and reopenings of the Panamanian Seaway (10)—and led to a strong increase in global ice volume and a global sea-level fall to up to 60 m below present-day values (60). As a consequence, global SST decreased by 2–3 K (59), with a 1–2 K decrease in the tropics (61); see Fig. 3 *C* and *F*. This low-latitude cooling could be related to the reduced dust flux offshore of Northwest Africa but can hardly explain the much earlier signature in the Arabian Sea.

A second possible triggering mechanism is the successive northward displacement of New Guinea, because of which in-

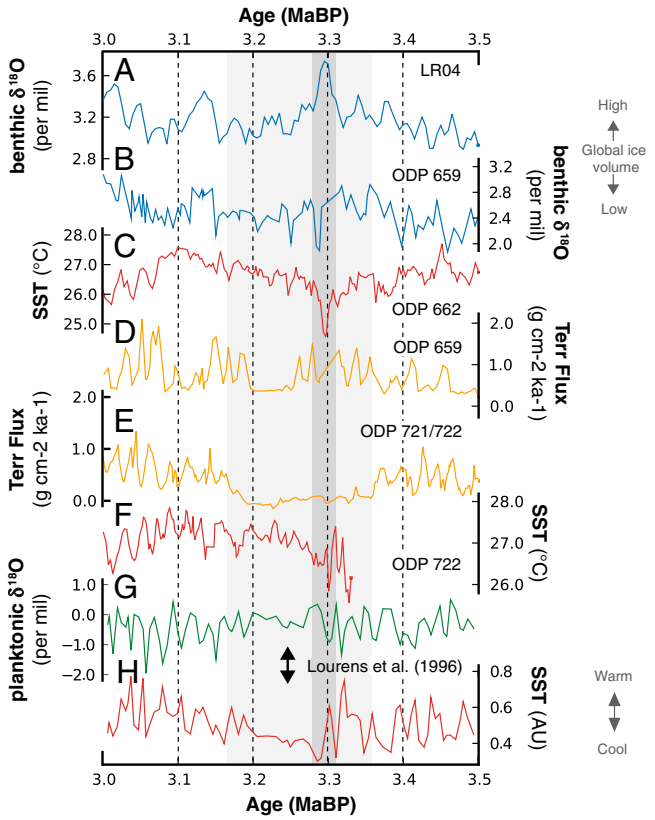

Fig. 3. Comparison of Middle Pliocene (3.5–3.0 Ma B.P.) global ice volume, sea-surface temperature, and dust flux reconstructions: (*A*) δ^{18}O benthic stack record LR04 (57); (*B*) benthic δ^{18}O record from ODP site 659; (*C*) alkenone-based SST reconstruction from ODP site 662 (61); (*D*) terrigenous dust flux at ODP site 659 (34); (*E*) terrigenous dust flux at ODP site 721/722 (1, 2); (*F*) alkenone-based SST reconstruction from ODP site 722 (61); (*G*,*H*) planktonic δ^{18}O and SST reconstruction from ensembles of planktonic foraminifera for a composite sequence from Southern Italy (69). The dark gray vertical bar indicates the MIS M2 (preceding an epoch with cold SST in the Mediterranean Sea and reduced dust flux into the Atlantic Ocean); the light gray bar indicates the interval of reduced dust flux into the Arabian Sea.

stead of warmer Equatorial Pacific water presently only less saline and colder North Pacific water can pass the Indonesian throughflow (62). Recent paleoceanographic reconstructions revealed that, during the Pliocene, subsurface waters in the eastern tropical Indian Ocean freshened and cooled by about 4 K, including a major cooling step between 3.5 and 2.95 Ma B.P. (63). Although SST was much less affected in most parts of the Indian Ocean, the southern coast of the Arabian Peninsula as well as the region around the horn of Africa are known as (wind-driven seasonal) upwelling regions (61, 64), which suggests that cold subsurface waters could have (at least intermittently) reached the ocean surface in this area and, thus, have led to a considerable decrease in the average regional SST. Recent alkenone-based SST reconstructions for ODP site 721/722 (61) actually confirm strong SST variations with partially extremely low values between at least 3.33 (the beginning of the respective record) and 3.28 Ma B.P. (see Fig. 3*F*), which cannot be explained by the known pattern of early glacial activity (57).

In summary, both aforementioned factors would have led to decreasing SSTs and, hence, to lower surface air temperatures and potential changes in the evaporation-precipitation balance. As a consequence, less convective rainfall, but also a shift (and possible weakening) of dominating atmospheric circulation patterns, was likely. Because in the potential source areas of terrigenous dust lower temperatures foster the formation of a closed vegetation cover, erosion and, hence, dust mobilization would have decreased. This interpretation is supported by the existence of large lakes in East Africa between 3.4 and 2.95 Ma B.P. [including the most pronounced lake episode in the Afar region (65) at about 3.33–3.23 Ma B.P.] pointing towards a very humid climate (Fig. 2*D*). Our considerations above are speculative so far and need confirmation from modeling studies and complementary paleoclimate archives.

Climate Variability and Human Evolution. To study the influence of African climate variability on human evolution, we compare the major large-scale transitions in African climate identified above with the currently available fossil record (Fig. 2*E*). Particularly, we observe that transitions in hominin evolution indicated by the appearance and disappearance of hominin species tend to cluster close to the identified climate shifts. These observed coincidences are unlikely to arise by chance even when taking into account dating uncertainties and the inherent incompleteness of the fossil record, as can be shown by using a suitable statistical significance test (*SI Text*).

The presented results therefore shed some light on the possible interrelationships between long-term climate change and hominin evolution. Specifically, we suggest that shifts between periods of more regular and more erratic environmental variability have been particularly important triggers for the development of humankind in East Africa. On the one hand, epochs of higher regularity could have led to stabilization and gradual increase of a population and, thus, a spread of a species over a larger area. On the other hand, subsequent periods of more irregular climate variability, possibly associated with changes in long-term trends, would have created an additional evolutionary pressure via a fragmentation of habitats and, thus, adaptation and diversification leading to speciation (18).

Supporting and extending Potts' variability selection hypothesis on environmental control of human evolution (23, 24), our point of view strongly suggests that, in addition to the mean climate conditions and the amplitude of variations of environmental parameters, (intermittent) changes in the regularity of climate fluctuations should be considered in future, more refined theories. In line with Potts' hypothesis, this mechanism on orbital time scales would benefit generalists like *Homo*, which are able to cope with strongly varying environmental conditions, but penalize specialists like *Paranthropus* (23). We must, however, keep in mind that the time scales of variations that are possibly relevant for migration of populations are not yet resolved in the available paleoclimate data. The necessity for further testing the extended variability selection hypothesis put forward here against other hypotheses (see the Introduction) calls for future efforts to obtain high-resolution (decadal to centennial scale) data on Plio-Pleistocene African climate history.

Conclusions

The nonlinear technique employed in this study is able to unravel large-scale changes in the temporal variability of African environmental conditions on supermillennial time scales. Comparing our results with findings from linear studies (17) demonstrates that past climate change in Africa includes a significant, previously overlooked nonlinear component. This complementary information supports the conclusions of ref. 17 in that we do not find evidence for sustained and irreversible step-like changes in climate variability that were proposed by refs. 1 and 2.

Our results provide clear evidence for subtle, but significant, transitions in the dynamics of mineral dust transport from the African continent to the adjacent oceans at about 3.35–3.15, 2.25–1.6, and 1.1–0.7 Ma B.P. These transitions unanimously correlate with important global climate transitions, such as changing ocean circulation (after 3.5 Ma B.P.), the intensification of the low-latitude Walker Circulation (*ca.* 1.7 Ma B.P.), and the onset of 100-ka glacial-interglacial cycles during the Middle Pleistocene

transition (*ca.* 1.25–0.7 Ma B.P.). The three episodes are characterized by radical changes in the ocean-atmosphere conditions, and hence the timing, magnitude, and style of wet-dry-wet transitions in tropical and subtropical Africa, without doubt influencing the regional climate and environment of early humans.

Indeed, we observe statistically significant coincidences between the detected climate shifts and transitions in human evolution in the geological record. By analogy, this link may be regarded as a warning considering the large risks for future human societies associated with climate tipping elements undergoing potentially irreversible, qualitative transitions due to anthropogenic climate change during the 21st century, even if the time scales involved are very different. To harness the potential of RN analysis and other nonlinear techniques to provide early warning of climate tipping points on these centennial time scales remains a challenge for future research.

Materials and Methods

The terrigenous dust flux records from ODP sites 659 (Atlantic Ocean offshore West Africa) (34), 721/722 (Arabian Sea) (1, 2), and 967 (Eastern Mediterranean Sea) (66) (see Fig. 2) allow reconstruction of North African dust mobilization and transport over the past 5 Ma and, hence, encode temporal changes in both the aridity of the region and the strength and direction of dominant regional atmospheric circulation patterns (17). We chose these records because they are well studied in the literature (1, 2, 17, 34, 66) and are at the same time representatively distributed around North Africa. Terrigenous dust flux has been estimated by using different approaches: from the relative abundance of the noncarbonate fraction and the dry-bulk density for site 659, via linear regression from the magnetic susceptibility (which can be measured much more easily) for site 721/722 (67), to artificially induced magnetic remanescence for site 967 (for more details, see ref. 17).

ACKNOWLEDGMENTS. Discussions with M. Schulz, N. Schütz, M. Mudelsee, H. von Suchodoletz, J. Heitzig, and K. Rehfeld provided valuable ideas to this work. We thank R. Grzondziel and C. Linstead for help with the IBM iDataPlex Cluster at the Potsdam Institute for Climate Impact Research and A. Schlums for proofreading of this manuscript. Complex network measures have been partly calculated by using the software package igraph (68). This work has been financially supported by the Deutsche Forschungsgemeinschaft (DFG) research group 1380 "Himalaya: Modern and Past Climates" (HIMPAC), the Leibniz Association (project ECONS: Evolving Complex Networks), the Federal Ministry for Education and Research via the Potsdam Research Cluster for Georisk Analysis, Environmental Change and Sustainability (PROGRESS), and the DFG Graduate School of Earth Sciences (GRK 1364 "Interactions between Tectonics, Climate and the Biosphere in the African-Asian Monsoonal Region"). J.F.D. acknowledges financial support by the German National Academic Foundation.

1. deMenocal PB (1995) Plio-Pleistocene African climate. *Science* 270:53–59.
2. deMenocal PB (2004) African climate change and faunal evolution during the Pliocene-Pleistocene. *Earth Planet Sci Lett* 220:3–24.
3. Trauth MH, et al. (2007) High- and low-latitude forcing of Plio-Pleistocene East African climate and human evolution. *J Hum Evol* 53:475–486.
4. deMenocal PB (2011) Climate and human evolution. *Science* 331:540–542.
5. Clemens S, Prell W, Murray D, Shimmield G, Weedon G (1991) Forcing mechanisms of the Indian Ocean monsoon. *Nature* 353:720–725.
6. Trauth MH, Deino AL, Bergner AG, Strecker MR (2003) East African climate change and orbital forcing during the last 175 kyr BP. *Earth Planet Sci Lett* 206:297–313.
7. Trauth MH, Maslin MA, Deino A, Strecker MR (2005) Late Cenozoic moisture history of East Africa. *Science* 309:2051–2053.
8. Haug GH, Tiedemann R (1998) Effect of the formation of the Isthmus of Panama on Atlantic Ocean thermohaline circulation. *Nature* 393:673–676.
9. Bartoli G, et al. (2005) Final closure of Panama and the onset of Northern Hemisphere glaciation. *Earth Planet Sci Lett* 237:33–44.
10. Sarnthein M, et al. (2009) Mid-Pliocene shifts in ocean overturning circulation and the onset of quaternary-style climates. *Climate Past* 5:269–283.
11. Ravelo A, Andreasen D, Lyle M, Lyle A, Wara M (2004) Regional climate shifts caused by gradual global cooling in the Pliocene epoch. *Nature* 429:263–267.
12. Berger W, Jansen E (1994) *The Polar Oceans and Their Role in Shaping the Global Environment*, Geophysical Monograph, eds OJR Muench and J Overland (American Geophysical Union, Washington), Vol 85, pp 295–311.
13. Mudelsee M, Schulz M (1997) The Mid-Pleistocene climate transition: Onset of 100 ka cycle lags ice volume build-up by 280 ka. *Earth Planet Sci Lett* 151:117–123.
14. Kutzbach JE, Streetperrott FA (1985) Milankovitch forcing of fluctuations in the level of tropical lakes from 18 to 0 kyr BP. *Nature* 317:130–134.
15. Kutzbach JE, Liu Z (1997) Response of the African monsoon to orbital forcing and ocean feedbacks in the middle Holocene. *Science* 278:440–443.
16. Ruddiman W (2008) Book review: Human environments in the East African Pliocene: An assessment of the faunal evidence. *EOS Trans AGU* 89:145.
17. Trauth MH, Larrasoaña JC, Mudelsee M (2009) Trends, rhythms and events in Plio-Pleistocene African climate. *Quat Sci Rev* 28:399–411.
18. Trauth MH, et al. (2010) Human evolution in a variable environment: The amplifier lakes of Eastern Africa. *Quat Sci Rev* 29:2981–2988.
19. Reynolds SC, Bailey GN, King GCP (2011) Landscapes and their relation to hominin habitats: Case studies from Australopithecus sites in eastern and southern Africa. *J Hum Evol* 60:281–298.
20. Darwin C (1859) *On the Origin of Species by Means of Natural Selection* (John Murray, London).
21. Vrba E (1985) Environment and evolution: Alternative causes of the temporal distribution of evolutionary events. *S Afr J Sci* 81:229–236.
22. Vrba E (1993) The pulse that produced us: Two major global coolings may have prodded antelopes and humans to evolve: How did humans get that way? *Natural History* 102:47–51.
23. Potts R (1996) Evolution and climate variability. *Science* 273:922–923.
24. Potts R (1998) Environmental hypotheses of hominin evolution. *Yearb Phys Anthropol* 41:93–136.
25. Maslin M, Trauth M (2009) *The First Humans—Origins of the Genus Homo*, eds F Grine, R Leakey, and J Fleagle (Springer, New York), 151–158.
26. Xu X, Zhang J, Small M (2008) Superfamily phenomena and motifs of networks induced from time series. *Proc Natl Acad Sci USA* 105:19601–19605.
27. Donner RV, Zou Y, Donges JF, Marwan N, Kurths J (2010) Recurrence networks—A novel paradigm for nonlinear time series analysis. *New J Phys* 12:033025.
28. Donner RV, et al. (2011) Recurrence-based time series analysis by means of complex network methods. *Int J Bifurcat Chaos* 21:1019–1046.
29. Donges JF, et al. (2011) Identification of dynamical transitions in marine palaeoclimate records by recurrence network analysis. *Nonlin Processes Geophys* 18:545–562.
30. Marwan N, Donges JF, Zou Y, Donner RV, Kurths J (2009) Complex network approach for recurrence analysis of time series. *Phys Lett A* 373:4246–4254.
31. Newman M (2003) The structure and function of complex networks. *SIAM Rev* 45:167–256.
32. Zou Y, Donner RV, Donges JF, Marwan N, Kurths J (2010) Identifying complex periodic windows in continuous-time dynamical systems using recurrence-based methods. *Chaos* 20:043130.
33. Prospero J, Ginoux P, Torres O, Nicholson S, Gill T (2002) Environmental characterization of global sources of atmospheric soil dust identified with the Nimbus 7 Total Ozone Mapping Spectrometer (TOMS) absorbing aerosol product. *Rev Geophys* 40:1002.
34. Tiedemann R, Sarnthein M, Shackleton NJ (1994) Astronomic timescale for the Pliocene Atlantic δ^{18}O and dust flux records of Ocean Drilling Program Site 659. *Paleoceanography* 9:619–638.
35. Clemens SC, Murray DW, Prell WL (1996) Nonstationary phase of the P1io-Pleistocene Asian monsoon. *Science* 274:943–948.
36. Lenton TM, et al. (2008) Tipping elements in the Earth's climate system. *Proc Natl Acad Sci USA* 105:1786–1793.
37. Schellnhuber HJ (2009) Tipping elements in the Earth system. *Proc Natl Acad Sci USA* 106:20561–20563.
38. Levermann A, et al. (2011) Potential climatic transitions with profound impact on Europe. *Clim Change*, (in press).
39. Lenton TM (2011) Early warning of climate tipping points. *Nat Clim Chang* 1:201–209.
40. Kuehn C (2011) A mathematical framework for critical transitions: Bifurcations, fast-slow systems and stochastic dynamics. *Physica D* 240:1020–1035.
41. Thompson JMT, Sieber J (2011) Predicting climate tipping as a noisy bifurcation: A review. *Int J Bifurcat Chaos* 21:399–423.
42. Held H, Kleinen T (2004) Detection of climate system bifurcations by degenerate fingerprinting. *Geophys Res Lett* 31:L23207.
43. Livina VN, Lenton TM (2007) A modified method for detecting incipient bifurcations in a dynamical system. *Geophys Res Lett* 34:L03712.
44. Dakos V, et al. (2008) Slowing down as an early warning signal for abrupt climate change. *Proc Natl Acad Sci USA* 105:14308–14312.
45. Scheffer M, et al. (2009) Early-warning signals for critical transitions. *Nature* 461:53–59.
46. Scheffer M (2009) *Critical Transitions in Nature and Society* (Princeton Univ Press, Princeton).
47. Donner RV, Heitzig J, Donges JF, Zou Y, Kurths J (2009) The geometry of chaotic dynamics—A complex network perspective. *Eur Phys J B*, (in press).
48. Donner R, Witt A (2006) Characterisation of long-term climate change by dimension estimates of multivariate palaeoclimatic proxy data. *Nonlin Processes Geophys* 13:485–497.
49. Livina VN, Kwasniok F, Lenton TM (2010) Potential analysis reveals changing number of climate states during the last 60 kyr. *Climate Past* 6:77–82.
50. Thompson JMT, Sieber J (2011) Climate tipping as a noisy bifurcation: A predictive technique. *IMA J Appl Math* 76:27–46.
51. Clark PU, et al. (2006) The middle Pleistocene transition: characteristics, mechanisms, and implications for long-term changes in atmospheric pCO_2. *Quat Sci Rev* 25:3150–3184.
52. Haywood A, Dekens P, Ravelo A, Williams M (2005) Warmer tropics during the mid-Pliocene? Evidence from alkenone paleothermometry and a fully coupled ocean-atmosphere GCM. *Geochem Geophys Geosys* 6:Q03010.
53. Solomon S, et al. (2007) *Contribution of Working Group I to the Fourth Assessment Report of the Intergovernmental Panel on Climate Change* (Cambridge Univ Press, Cambridge).

54. Robinson MM (2009) New quantitative evidence of extreme warmth in the Pliocene Arctic. *Stratigraphy* 6:265–275.
55. Dowsett HJ, Robinson MM, Foley KM (2009) Pliocene three-dimensional global ocean temperature reconstruction. *Climate Past* 5:769–783.
56. Shackleton N, Hall M, Pate D (1995) Pliocene stable isotope stratigraphy of site 846. *Proc Ocean Drill Prog Sci Results* 138:337–355.
57. Lisiecki L, Raymo M (2005) A Pliocene-Pleistocene stack of 57 globally distributed benthic δ^{18}O records. *Paleoceanography* 20:PA1003.
58. Steph S, et al. (2006) Changes in Caribbean surface hydrography during the Pliocene shoaling of the Central American Seaway. *Paleoceanography* 21:PA4221.
59. deSchepper S, Head MJ, Groeneveld J (2009) North Atlantic Current variability through marine isotope stage M2 (circa 3.3 Ma) during the mid-Pliocene. *Paleoceanography* 24:PA4206.
60. Dwyer GS, Chandler MA (2009) Mid-Pliocene sea level and continental ice volume based on coupled benthic Mg/Ca palaeotemperatures and oxygen isotopes. *Philos Transact A Math Phys Eng Sci* 367:157–168.
61. Herbert TD, Peterson LC, Lawrence KT, Liu Z (2010) Tropical ocean temperatures over the past 3.5 million Years. *Science* 328:1530–1534.
62. Cane MA, Molnar P (2001) Closing of the Indonesian seaway as a precursor to east African aridification around 3–4 million years ago. *Nature* 411:157–162.
63. Karas C, et al. (2009) Mid-Pliocene climate change amplified by a switch in Indonesian subsurface throughflow. *Nat Geosci* 2:434–438.
64. Schils T, Coppejans E (2003) Phytogeography of upwelling areas in the Arabian Sea. *J Biogeogr* 30:1339–1356.
65. Campisano CJ, Feibel CS (2007) Connecting local environmental sequences to global climate patterns: Evidence from the hominin-bearing Hadar Formation, Ethiopia. *J Hum Evol* 53:515–527.
66. Larrasoaña JC, Roberts AP, Rohling EJ, Winklhofer M, Wehausen R (2003) Three million years of monsoon variability over the northern Sahara. *Clim Dyn* 21:689–698.
67. Bloemendal J, deMenocal P (1989) Evidence for a change in the periodicity of tropical climate cycles at 2.4 Myr from whole-core magnetic susceptibility measurements. *Nature* 342:897–900.
68. Csárdi G, Nepusz T (2006) The igraph software package for complex network research. *InterJournal Complex Systems* CX.18:1695.
69. Lourens L, et al. (1996) Evaluation of the Plio-Pleistocene astronomical timescale. *Paleoceanography* 11:391–413.
70. Hailemichael M, Aronson J, Savin S, Tevesz M, Carter J (2002) δ^{18}O in mollusk shells from Pliocene Lake Hadar and modern Ethiopian lakes: Implications for history of the Ethiopian monsoon. *Palaeogeogr Palaeoclimatol Palaeoecol* 186:81–99.

Supporting Information

Donges et al. 10.1073/pnas.1117052108

SI Text

Recurrence Network Analysis of Time Series. ***Windowed analysis.*** To detect dynamical transitions in a time series $d(t)$, we view this series through a sliding window of W data points with a step size of ΔW data points. The data within the μ-th window, $x(t) = d(t)|_{t=t_i}$, $i = \mu\Delta W,\ldots,\mu\Delta W + W$, are analyzed separately thereafter. Because of the widely differing average sampling times $\langle\Delta T\rangle$ of all three records (ODP site 659: $\langle\Delta T\rangle_1 = 4.10$ ka, ODP site 721/722: $\langle\Delta T\rangle_2 = 1.81$ ka, ODP site 967: $\langle\Delta T\rangle_3 = 0.36$ ka), and to avoid interpolation, we prescribe the desired average window size W^* in units of time. This approach guarantees that all three records are viewed at a comparable time scale. Our choice of $W^* = 410$ ka is guided by the trade-off between high temporal resolution (small W^*) and statistical confidence (large W^*), but the results are robust within a reasonable range of W^* (1). The windows of $W = \lfloor W^*/\langle\Delta T\rangle \rfloor$ data points then cover approximately W^* years, with deviations of maximum 44% due to irregular sampling. We choose a window overlap of 90%, resulting in a step size of approximately $\Delta W^* = 41$ ka, $\Delta W = \lfloor \Delta W^*/\langle\Delta T\rangle \rfloor$, and maximum deviations of 97%. For every record, the number of data points W in all windows is kept constant (rather than window size in the time domain). Thereby we assure that even extensive statistics (i.e., quantitative measures that do explicitly depend on the number of considered data points) show comparable results along each time series. However, because of the different sampling rates, the choice of a consistent reference time scale W^* for all records requires different choices of W, specifically, $W_1 = 100$ for ODP site 659, $W_2 = 226$ for site 721/722, and $W_3 = 1139$ for site 967, which implies that results from different records should be compared qualitatively only. This limitation does not impact the comparability of the timing of events, because the window lengths all correspond to the reference time scale W^* and we furthermore use the window's midpoints to attach a timing to the recurrence network measures obtained from a particular window (see below).

Embedding of time series. Next, we unfold each time series segment (window) $x(t)$ by time-delay embedding to obtain a vector valued trajectory $\mathbf{x}(t) = \{x(t), x(t+\tau),\ldots,x(t+(m-1)\tau)\}$ (2, 3). The embedding dimension $m = 3$ presents a reasonable compromise given the relatively short time series and the underlying high-dimensional dynamics as suggested by the false nearest neighbor criterion (4, 5). We choose the delay τ to cover approximately the same time scale for all three considered records, i.e., $\tau = \lfloor \tau^*/\langle\Delta T\rangle \rfloor$ with $\tau^* = 10$ ka, corresponding to the order of the decorrelation time for all three time series (1). The result is $\tau_1 = 2$ time steps for ODP site 659, $\tau_2 = 5$ for site 721/722, and $\tau_3 = 27$ for site 967. A detailed discussion of the limitations of this approach with respect to the irregular sampling of the considered time series is given in a complementary technical paper (1).

Recurrence network construction. To represent the recurrence structure within the current time window, we construct an ε-recurrence network (RN) from $\mathbf{x}(t)$ (5–8). The nodes i of this complex network (9, 10) are the W state vectors $\mathbf{x}_i = \mathbf{x}(t = t_i)$ embedded in the m-dimensional reconstructed phase space corresponding to times t_i. We link two nodes i and j if the associated states are very similar—i.e., $\mathbf{x}_i \approx \mathbf{x}_j$. The network's adjacency matrix A_{ij} (9) is given by

$$A_{ij} = \Theta(\varepsilon - \|\mathbf{x}_i - \mathbf{x}_j\|) - \delta_{ij}, \qquad \text{[S1]}$$

where $\Theta(\cdot)$ is the Heaviside function, $\|\cdot\|$ the maximum norm, ε the recurrence threshold, and δ_{ij} the Kronecker delta introduced to exclude self-loops (7). ε is chosen adaptively for each window to guarantee a reasonable choice of the link density fixed at approximately 5% (7, 11). RNs are closely linked with the established concept of recurrence quantification analysis (12), which has been previously used in the context of paleoclimate time series analysis (13, 14).

Network measures and interpretation. So far we have obtained a complex network for each window describing the dust flux dynamics during the associated epoch in the past. We now proceed to quantitatively characterize these networks in terms of two conceptually different graph-theoretic measures (9, 10), which are both sensitive to dynamical transitions in time series mapped to RNs (5, 8, 15). We consider the transitivity properties captured by the measure *network transitivity* (9, 10)

$$\mathscr{T} = \frac{\sum_{i,j,k} A_{ij}A_{jk}A_{ki}}{\sum_{i,j,k} A_{ki}A_{kj}}. \qquad \text{[S2]}$$

$\mathscr{T}$ is larger for regular and smaller for more irregular dynamics within the considered time series segment (5, 8, 15). The *average path length*

$$\mathscr{L} = \langle l_{ij}\rangle_{ij} \qquad \text{[S3]}$$

gives the mean value of the minimum number of links l_{ij} (geodesic graph distance) that have to be crossed to get from node i to j in the RN (9), where $\langle\cdot\rangle_{ij}$ denotes an average over all pairs of nodes. The average is taken only over pairs of nodes that belong to the same network component (i.e., which are mutually reachable on the graph). It tends to fluctuate strongly when the window slides across a dynamical transition (5, 8, 15), because the overall network structure often undergoes a qualitative change at such a point [e.g., because of the merging of two formerly disconnected network clusters (5)].

We use the window's midpoint for plotting the time evolution of $\mathscr{T}$ and $\mathscr{L}$ (see Fig. 2, main text). A notable advantage of our methodology is its insensitivity to changes in the age model underlying $x(t)$. As long as only the time points t_i, but not the actual data $x_i = x(t = t_i)$ (e.g., because of interpolation), differ between age models, our results will remain the same. Note that the only implicit assumption made here is that the available state vectors $\mathbf{x}_i$ in a given time window represent the distribution of states within this window with sufficiently high statistical confidence.

Significance test. Finally, we perform a significance test to ascertain at which times $\mathscr{T}$ and $\mathscr{L}$ deviate significantly from their expected values given the recurrence structure of the whole time series and window size W (8). The corresponding null hypothesis is that the network measures observed for a certain window are consistent with being calculated from a random draw of W state vectors from the prescribed phase space distribution induced by the entire time series. In order to create an appropriate null model, we use the following approach: (*i*) Draw randomly W state vectors from the embedded time series (corresponding to the chosen window size), (*ii*) construct a RN from this set of state vectors, and (*iii*) calculate the network measures of interest.

We obtain a test distribution for each of the network measures and time series separately from 100,000 realizations of this null model. Finally we estimate confidence bands bounded by the test distribution's 5% and 95% quantiles. This simple approach yields a test for stationarity on the basis of the structural features of RNs, where network measures significantly deviating from the empirical test distribution indicate epochs that include potential dynamical regime shifts.

Contemplating Coincidences. ***Introduction.*** We are concerned with the statistical problem of testing for coincidences of two distinct types of events: (*i*) shifts in climate (C events) and (*ii*) the appearance and disappearance of species in the fossil record (S events). Consider a record of N S events $S_1,\ldots,S_N$ and M C events $C_1,\ldots,C_M$ over a time period T, where both sequences are not necessarily ordered chronologically. A single coincidence occurs if an S event falls within the temporal tolerance window of a C event—i.e., $|t_S - t_C| \leq \Delta T$, where t_S and t_C denote the timing of both events (Fig. S1).

Assume that we observe in our record K_e single coincidences. Given these findings and considering the uncertainties in the timing of both types of events as well as the inherent incompleteness of the fossil record, we ask the following questions: Are the observed numbers of coincidences likely to have arisen by pure chance? Can we derive a significance test by combinatorial reasoning?

Statistical null model. Our null hypothesis is that both S and C events are distributed randomly, independently and uniformly over the time interval T. Furthermore, we assume that $\Delta T \ll T/M \ll T$. On the basis of these assumptions, the probability of a specific S event S_i falling into the tolerance window of a specific C event C_j is

$$p = 2\frac{\Delta T}{T}. \qquad \textbf{[S4]}$$

Then the probability of a specific S event S_i coinciding with *at least one* of the M C events is given by

$$1-(1-p)^M = 1-\left(1-2\frac{\Delta T}{T}\right)^M. \qquad \textbf{[S5]}$$

Now we are in a position to compute the probability $P(K;N,1-(1-p)^M)$ that exactly K single coincidences are observed for a given realization of the fully random null model. Because S events are assumed to be distributed independently in the interval $[0,T]$, $P(K;N,1-(1-p)^M)$ is the binomial distribution with N trials and success probability $1-(1-p)^M$ (16) yielding

$$P(K;N,1-(1-p)^M) = \binom{N}{K}\left[1-\left(1-2\frac{\Delta T}{T}\right)^M\right]^K \times \left[\left(1-2\frac{\Delta T}{T}\right)^M\right]^{N-K}. \qquad \textbf{[S6]}$$

From this distribution [Eq. **S6**] we easily derive the expectation value $\langle K\rangle$ and standard deviation $\sigma(K)$ as

$$\langle K\rangle = N[1-(1-p)^M] = N\left[1-\left(1-2\frac{\Delta T}{T}\right)^M\right] \qquad \textbf{[S7]}$$

and

$$\sigma(K) = \sqrt{N[1-(1-p)^M](1-p)^M} = \sqrt{N\left[1-\left(1-2\frac{\Delta T}{T}\right)^M\right]\left(1-2\frac{\Delta T}{T}\right)^M}. \qquad \textbf{[S8]}$$

The p value of an observation K_e with respect to the test distribution [Eq. **S6**]—i.e., the probability to obtain a number of coincidences K larger or equal to the empirically observed number K_e—is then given by

$$P(K \geq K_e) = \sum_{K^*=K_e}^{N} P(K^*;N,1-(1-p)^M). \qquad \textbf{[S9]}$$

Application. Our record of interest spans a time period of $T = 5$ Ma and contains $M = 6$ climate shifts (C events) as well as $N = 2\times 18+1 = 37$ S events (note that *Homo sapiens* is not extinct yet). In Fig. 2 (main text), significant shifts in African climate (C events) are marked by the upper and lower bounds of the gray bars spanning all data and results shown. Coincidences with the time of species appearance and disappearance (S events) considering a temporal tolerance of $\Delta T = 0.1$ Ma are marked by red bars.

The C events occur at approximately 3.5, 2.95, 2.25, 1.6, 1.1, and 0.7 Ma B.P. (Table S1), whereas the timings of all considered S events are listed in Table S2. Given a tolerance $\Delta T = 0.1$ Ma, we observe $K_e = 15$ single coincidences (Fig. 2, main text). This particular choice of the tolerance parameter ΔT is motivated by (*i*) the fact that the timings of most of the considered C and S events have been rounded to the first decimal point prior to the analysis, and (*ii*) uncertainties in dating of the analyzed dust flux records, the detected climate shifts, and hominin fossils which can be assumed to be roughly of this order.

We now aim to quantify the significance of the observed number of coincidences K_e with respect to the null model formulated above—i.e., assuming that both C and S events are distributed uniformly and independently within the time interval of interest. The null model yields an expected number of $\langle K\rangle = 8.04$ coincidences with the standard deviation $\sigma(K) = 2.51$ and the empirical observation corresponding to a p value of $P(K \geq K_e) = 0.003$. The change of p values $P(K \geq K_e)$ and the observed number of coincidences K_e with varying tolerance ΔT is shown in Fig. S2.

Discussion. Our analysis reveals that the observed number of coincidences is robustly significant with p values $P(K \geq K_e) \ll 0.05$ for a range of tolerance parameters $0.05 \leq \Delta T \leq 0.17$ with respect to the fully random null model (Fig. S2*A*). Considerably larger ΔT do not meet the basic assumption $\Delta T \ll T/M \ll T$ any more. In this sense the analysis supports a statement like the following: *The observed coincidences between detected climate shifts and the appearance or disappearance of hominin species are unlikely to arise by chance.* We should emphasize here that coincidence alone, like correlation, does not imply causality (17). It can only serve as a hint at a possible causal relationship.

Note that it is known that the appearance and/or disappearance of different species is typically correlated. This effect is not included in the null model but could be assessed with the help of more sophisticated Monte Carlo simulations. The proposed null model should be seen as the simplest possible quantitative means to justify discussing the influence of Plio-Pleistocene climate change on hominin evolution in the first place.

The presented statistical analysis assumes that the life spans of hominin species are approximated by the times to which their known fossils are dated, an assumption which is also routinely

relied upon in the reconstruction of hominin evolutionary trees or dispersal patterns (18). Minor dating uncertainties and fossil sampling effects are covered by the tolerance parameter ΔT. However, as is always the case in paleontological research, new fossil evidence may dramatically alter the current view of events in hominin evolution summarized in Table S2 (18). Furthermore taphonomic biases and sampling effects may play a significant role (17). Given new evidence, the proposed statistical framework will allow future investigators to quickly evaluate the significance of observed coincidences between C and S events. The same is true if the timing or number of climate shifts were to be revised. Our null model may moreover prove useful to test and compare other hypotheses relating changes in climate to evolutionary events.

Finally it is important to stress that the proposed significance test is asymmetric with respect to C and S events, which is mathematically expressed by the fact that Eq. **S6** is asymmetric with respect to the numbers of events M and N. Above we were concerned with the clustering of S events around C events, thereby implicitly testing for a potential causal influence of C events on S events and *not* vice versa. Considering the research question under study this assumption seems reasonable, because humans are not thought to have had a significant influence on continental and larger scale climate change before a few thousand years ago (see, e.g., the early anthropogenic hypothesis (19)).

1. Donges JF, et al. (2011) Identification of dynamical transitions in marine palaeoclimate records by recurrence network analysis. *Nonlin Processes Geophys* 18:545–562.
2. Packard NH, Crutchfield JP, Farmer JD, Shaw RS (1980) Geometry from a time series. *Phys Rev Lett* 45:712–716.
3. Takens F (1981) in *Dynamical Systems and Turbulence, Warwick 1980*, Lecture Notes in Mathematics, eds Rand D, Young LS (Springer, New York), Vol. 898, pp. 366–381.
4. Kennel M, Brown R, Abarbanel H (1992) Determining embedding dimension for phase-space reconstruction using a geometrical construction. *Phys Rev A* 45:3403–3411.
5. Marwan N, Donges JF, Zou Y, Donner RV, Kurths J (2009) Complex network approach for recurrence analysis of time series. *Phys Lett A* 373:4246–4254.
6. Donner RV, Zou Y, Donges JF, Marwan N, Kurths J (2010) Ambiguities in recurrence-based complex network representations of time series. *Phys Rev E* 81:015101(R).
7. Donner RV, Zou Y, Donges JF, Marwan N, Kurths J (2010) Recurrence networks—A novel paradigm for nonlinear time series analysis. *New J Phys* 12:033025.
8. Donner RV, et al. (2011) Recurrence-based time series analysis by means of complex network methods. *Int J Bifurcat Chaos* 21:1019–1046.
9. Newman M (2003) The structure and function of complex networks. *SIAM Rev* 45:167–256.
10. Boccaletti S, Latora V, Moreno Y, Chavez M, Hwang DU (2006) Complex networks: Structure and dynamics. *Phys Rep* 424:175–308.
11. Schinkel S, Dimigen O, Marwan N (2008) Selection of recurrence threshold for signal detection. *Eur Phys J Spec Top* 164:45–53.
12. Marwan N, Romano MC, Thiel M, Kurths J (2007) Recurrence plots for the analysis of complex systems. *Phys Rep* 438:237–329.
13. Marwan N, Trauth MH, Vuille M, Kurths J (2003) Comparing modern and Pleistocene ENSO-like influences in NW Argentina using nonlinear time series analysis methods. *Climate Dynamics* 21:317–326.
14. Trauth MH, Bookhagen B, Marwan N, Strecker MR (2003) Multiple landslide clusters record Quaternary climate changes in the northwestern Argentine Andes. *Palaeogeogr Palaeoclimatol Palaeoecol* 194:109–121.
15. Zou Y, Donner RV, Donges JF, Marwan N, Kurths J (2010) Identifying complex periodic windows in continuous-time dynamical systems using recurrence-based methods. *Chaos* 20:043130.
16. Jaynes ET, Bretthorst GL (2003) *Probability Theory: The Logic of Science* (Cambridge Univ Press, Cambridge, UK).
17. deMenocal PB (1995) Plio-Pleistocene African climate. *Science* 270:53–59.
18. Strait D, Wood B (1999) Early hominid biogeography. *Proc Natl Acad Sci USA* 96:9196–9200.
19. Ruddiman WF (2007) The early anthropogenic hypothesis: Challenges and responses. *Rev Geophys* 45:RG4001.
20. Trauth MH, et al. (2007) High- and low-latitude forcing of Plio-Pleistocene East African climate and human evolution. *J Hum Evol* 53:475–486.
21. Bromage T, Schrenk F, Zonnefeld F (1995) Paleoanthropology of the Malawi Rift: An early hominid mandible from the Chiwondo Beds, northern Malawi. *J Hum Evol* 28:71–108.
22. Kimbel W, et al. (1996) Late Pliocene Homo and Oldowan tools from the Hadar Formation (Kada Hadar Member), Ethiopia. *J Hum Evol* 31:549–561.
23. Reed K (1997) Early hominid evolution and ecological change through the African Plio-Pleistocene. *J Hum Evol* 32:289–322.
24. White T (2002) in *The Primate Fossil Record*, ed Hartwig W (Cambridge Univ Press, Cambridge, UK), pp. 407–417.
25. Dunsworth H, Walker A (2002) in *The Primate Fossil Record*, ed Hartwig W (Cambridge Univ, Cambridge, UK), pp. 419–436.
26. McHenry H (2002) in *The Primate Fossil Record*, ed Hartwig W (Cambridge Univ Press, Cambridge, UK), pp. 401–406.
27. Antón S, Swisher C (2004) Early dispersals of Homo from Africa. *Ann Rev Anthropol* 33:271–296.
28. White T, et al. (2006) Asa Issie, Aramis and the origin of *Australopithecus*. *Nature* 440:883–889.

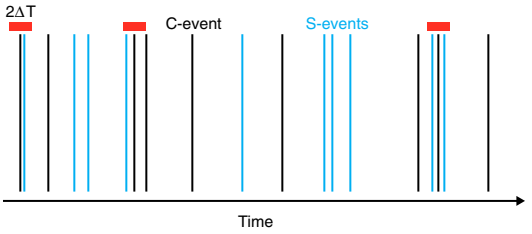

Fig. S1. Schematic representation of C events (black vertical lines) and S events (blue vertical lines). Red horizontal bars of length $2\Delta T$ centered around C events indicate coincidences of one or more S events with one C event. This choice leads to $K_e = 4$ coincidences in this example.

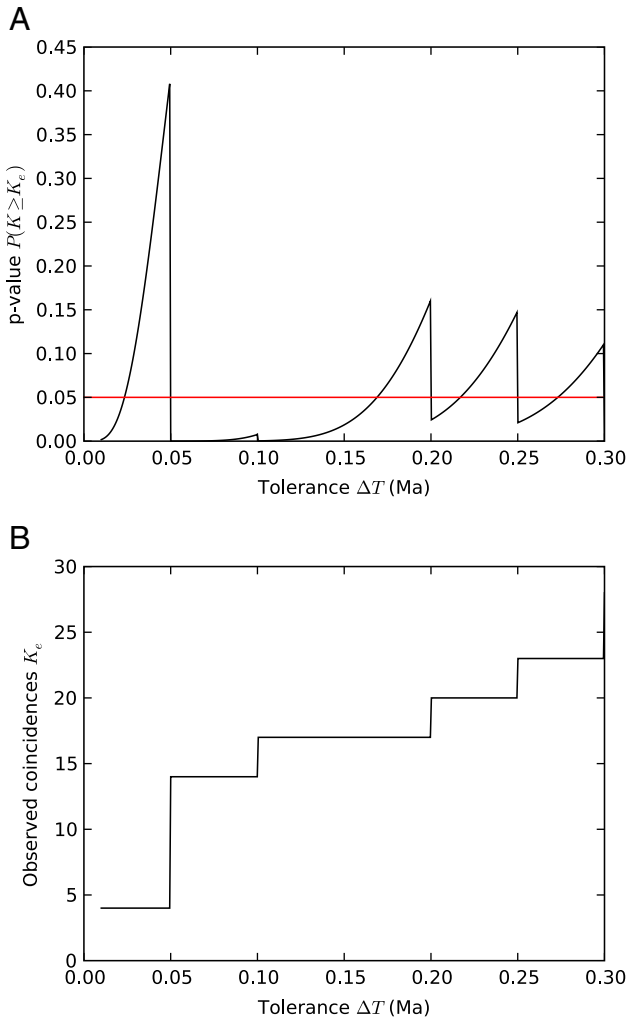

Fig. S2. (*A*) *P* values $P(K \geq K_e)$ of the (*B*) observed number of coincidences K_e for varying tolerance parameter ΔT. We consider the results to be significant if the *p* value is smaller than the commonly chosen significance level of 0.05 (red horizontal line).

Table S1. Timing of climate shifts identified by recurrence network analysis (see main text) and related paleoenvironmental change

Timing, Ma B.P.	Paleoenvironmental change
3.50	Appearance of lakes in EARS
2.95	Disappearance of large lakes in EARS
2.25	Reorganization of Walker circulation (beginning)
1.60	Reorganization of Walker circulation (end)
1.10	Middle Pleistocene transition (beginning)
0.70	Middle Pleistocene transition (end)

EARS, East African Rift System.

Table S2. Times of the appearance and disappearance of hominin species from the known fossil record taken from ref. 20, on the basis of refs. 21–28

Species	Appearance, Ma B.P.	Disappearance, Ma B.P.
Ardipithecus ramidus	4.55	4.40
Australopithecus anamensis	4.20	3.90
Kenyanthropus platyops	3.55	3.45
Australopithecus afarensis	3.60	2.90
Australopithecus bahrelghazali	3.55	3.45
Australopithecus africanus	3.00	2.50
Australopithecus garhi	2.55	2.50
Paranthropus aethiopicus	2.50	2.30
Paranthropus boisei	2.30	1.40
Homo habilis	2.30	1.60
Homo rudolfensis	2.30	1.60
Paranthropus robustus	1.90	1.10
Homo ergaster	1.90	1.00
Homo erectus	1.90	0.30
Homo antecessor	0.90	0.70
Homo heidelbergensis	0.60	0.10
Homo neanderthalensis	0.30	0.05
Homo floresiensis	0.10	0.05
Homo sapiens	0.16	-

The timing of most of these evolutionary S events has been rounded to the first decimal point.